ISSN NO. 2320-5407

*Journal homepage: http://www.journalijar.com*

*INTERNATIONAL JOURNAL OF ADVANCED RESEARCH*

**RESEARCH ARTICLE**

# A Systematic Study of High Energy Nuclear Collisions (light and heavy nuclei) by Simulations / Event Generators

***M. Ayaz Ahmad[1], M. Yassen. El-Bakry[1,2], Taymour A. Hamdalla[1,3], Mir Hashim Rasool[4] and Shafiq Ahmad[4]**

**1.** Department of Physics, Faculty of Science, P. O. Box 741, University of Tabuk, Tabuk, 71491, Saudi Arabia.
**2.** Department of physics, Faculty of Education, Ain Shams University, Roxy, Cairo, Egypt.
**3.** Department of Physics, Faculty of Science, Alexandria University, Alexandria , Egypt
**4.** Department of Physics, Aligarh Muslim University, Aligarh, 202002, India

**a.ahmad@ut.edu.sa,**

## *Manuscript Info*

***Manuscript History:***

Received: 11 November 2015
Final Accepted: 22 December 2015
Published Online: January 2016

***Key words:***
Quark–gluon plasma (QGP), Artificial Neural Network (ANN), Artificial Intelligence (AI), multiplicity correlation

****Corresponding Author***

**M. Ayaz Ahmad**

## *Abstract*

In the present article, we tried to draw some important features of the applicability test and the functioning effect of various nuclear models used in the relativistic nuclear collisions for hadrons-hadrons, hadron-nucleus and nucleus-nucleus interactions. The proposed models simulate the multiplicity distributions of the secondary charged particles produced in such collisions. The prediction capability of the artificial intelligence (AI) was checked by the experimental data which is not used in the simulation. Finally, it has been found that the artificial intelligence (AI) has the ability to simulate and predict the heavy ion collisions data.



## Introduction:-

Particle physics is the science of the fundamental structure of matter, which leads to the study of the properties of subatomic particles and the mechanism of their interactions. Its ultimate aim is to find a complete description of the elementary constituents of matter and of the forces acting between them, a description, which should be as simple as possible [1,2]. It is appropriate to study the field in terms of theoretical and the experimental points of view [3]. Theory predicts phenomenon, which can be verified by experiments, and experiments very often provide new insight through unexpected results, which in turn lead to the improvement in theoretical description [4].

The interest in the study of high-energy nuclear matter has increased many folds due to the possibility of studying unstable states of nuclear matter under extreme condition of high energy density and high temperature. It is generally believed that the strong interacting nuclear matter in these violent collisions may undergo phase transition under such conditions and this phenomenon may predict the formation of deconfined state of freely interacting quarks and gluons known as quark–gluon plasma (QGP), which is believed to have existed in the form of QGP for few microseconds after the Big Bang. In the later stage of collisions, the quark may interact to give rise to a large number of jets or clusters, finally resulting into large number of pions [1-4].

The Quantum Chromo Dynamics (QCD) theory describes the strong interactions between the hadronic matter which predicts a novel phase transition from a confined state of quark and gluon to de-confined state, where quarks and gluons would be free to move and freely interacting in the hadronic matter, which would be at higher energy density. No conclusive experimental evidence for the formation of QGP has been found in nucleus-nucleus collisions at low as well as ultra-relativistic energies [4-5].

In this article, an attempt has been made to study the general characteristics of heavily ionizing particles and relativistic shower particles produced in $^{28}$ Si - emulsion interactions at 14.6 A GeV. This will help to extract the valuable informations about the mechanism of multiparticle production. The multiplicity distribution of charged secondaries produced and their correlations have been studied using 973 interactions of silicon beam with emulsion nuclei. Angular distribution of shower particles has also been studied.

## Material and Methods:-

In the present experiment, FUJI nuclear emulsion pellicles were irradiated horizontally with a beam of $^{28}$Si nuclei at 14.6A GeV at Alternating Gradient Synchrophasotron (AGS) of Brookhaven National Laboratory (BNL), NewYork, USA. The scanning of the plates is performed with the help of Leica DM2500M microscope with a 10× objective and 10X ocular lens provided with semi-automatic scanning stages. The method of line scanning was used to collect the inelastic $^{28}$Si-Em interactions. The interactions collected from line scanning were scrutinized under an optical microscope (Semi-Automatic Computerized, Leica DM6000M) with a total magnification of 10 * 100 using 10X eyepiece and 100X oil immersion objective. The measuring system associated with it has 1 μm resolution along X and Y axes and 0.5 μm resolution along the Z-axis.

The tracks associated with the interactions are classified in accordance with their ionization, range and velocity [6], [7]. The tracks having specific ionization $g^*(=g/go) < 1.4$ and relative velocity $\beta > 0.7$ are taken as shower tracks, where *go* is the Fowler and Perkins parameter for plateau ionization of relativistic particles. The number of such tracks in an event is represented by "*NS*". Shower tracks producing particles are mostly pions, with small admixture of charged K-mesons and fast protons. The secondary tracks having specific ionization in the interval $1.4 < g^* \leq 10$ are known as grey tracks. The number of such tracks in a star is designated by "*Ng*". This corresponds to protons with velocity in the interval $0.3 \leq \beta \leq 0.7$ and range $\geq 3.0$ mm in emulsion. The present work is based on these shower tracks only. Grey tracks are associated with the recoiling protons and have energy range (30 - 400) MeV. The sum of the number of grey and shower tracks in such an interaction is known as compound particle multiplicity and their number in a collision is represented by $Nc = Ng + Ns$. Black tracks are mainly the fragments emitted from excited target. The secondary tracks having specific ionization $g^* > 10$ are classified as black tracks, which is represent by "*Nb*". This corresponds to protons of relative velocity $\beta < 0.3$ having a range in emulsion $R < 3.0$ mm. The particles producing black tracks are mainly the fragments emitted from the excited target. This ionization corresponds to protons with energy range < 30 MeV.

The black and grey tracks taken together are said to be heavily ionizing tracks. Thus these tracks correspond to $g^* \geq 1.4$ or $\beta \leq 0.7$. Their number in a star, $Nh = (Nb + Ng)$ is a characteristics of the target. There is a limitation with nuclear emulsion that the exact identification of target is not possible since the medium of the emulsion is heterogeneous and composed of H, C, N, O, Ag and Br nuclei. The events produced due to the collisions with different targets in nuclear emulsion are usually classified into three main categories on the basis of the multiplicity of heavily ionizing tracks in it [6-10].

In the present work we have categorized the events on the bases of *Nh* multiplicity as: The events with $N_h$ in range $2 \leq Nh \leq 7$ are classified as collision with group of light nuclei (CNO, $\langle A_T \rangle = 14$) and $N_h \geq 8$ are classified as collision with group of heavy nuclei (AgBr, $\langle A_T \rangle = 94$). And the events with all $N_h$ values are classified as collision with emulsion.

### Artificial Neural Networks (ANNS):-

Artificial Neural Network (ANN) is a general mathematical computing paradigm that models the operations of biological neural systems. ANN is a powerful general-purpose technique and they have been widely applied to a variety of physics problems, and in some fields such as high energy physics, they are the most widely applied computational intelligence technique.

ANNs are electrical analogues of the biological neural networks. Biological nerve cells, called neurons, receive signals from neighboring neurons or receptors through dendrites, process the received electrical pulses at the cell body and transmit signals through a large and thick nerve fiber, called an axon (See Figure 1). In a similar way, the electrical model of typical biological neuron consists of a linear activator, followed by a nonlinear inhibiting function [11]. The linear activation function yields the sum of the weighted input excitation, while the nonlinear inhibiting function attempts to culture the signal levels of the sum.

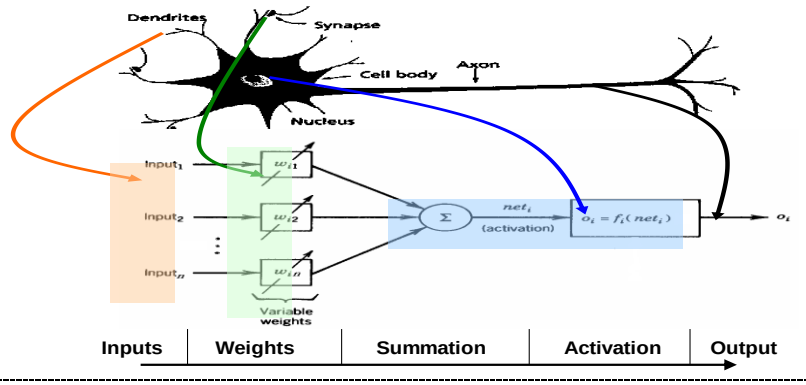


**Fig. 1.** A block diagram of Biological neuron versus artificial neurons.

An ANN is a collection of such electrical neurons connected in different topologies. The most common application of an ANN is in machine learning. In a learning problem, the weights and/or nonlinearities in an ANN undergo an adaptation (or learning) cycle. The adaptation cycle is required for updating these parameters of the network, until a state of equilibrium is reached. The ANN support both supervised and unsupervised types of machine learning. ANNs can be considered as simplified mathematical models of brain-like systems and they function as parallel-distributed computing networks. However, in contrast to conventional computers, which are programmed to perform specific task, most neural networks must be taught, or trained. They can learn new associations, new functional dependencies and new patterns. Neural networks obviate the need to use complex mathematically explicit formulas, computer models and impractical and costly physical models.

## The Mathematical Model:-

When creating a function model of the biological neuron, there are three basic components of importance. First, the synapses of the neuron are modeled as weights. The strength of the connection between an input and a neuron is noted by the value of the weight. Negative weight values reflect inhibitory connections, while positive values designate excitatory connections. The next two components model the actual activity within the neuron cell. An adder sums up all the inputs modified by their respective weights. This activity is referred to as linear combination. Finally, an activation function controls the amplitude of the neuron. An acceptable range of output is usually between 0 and 1, or -1 and 1. Mathematically, this process is described in the figure (2):

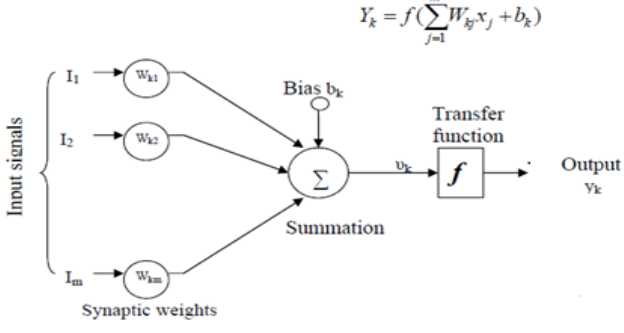


**Fig. 2.** Operation scheme of a typical artificial neural network.[12, 13]

From this model the interval activity of the neuron can be shown to be:

$$Y_k = f(\sum_{j=1}^{m} W_{kj} + b_k) \quad (1)$$

The output of the neuron, $Y_k$, would therefore be the outcome of some activation on the value of $v_k$. The hidden neurons (neurons of hidden layers) and the weight factors of the links between them play a critical role during the learning processing. In the case of supervised training, the numerical values of the weight factors change according to the training data sets, in order to minimize the difference between the actual outputs and the target values. Thus, the relationship between causal factors and response is mapped during the learning process. The transfer function of processing nodes is used to determine the output value of the node based on the total net input from nodes in prior layer. The most widely used transfer functions are a sigmoid and tan sigmoid function, which are shown in the following equations [11-13]:-

$$Y^{sigmoid} = \frac{1}{1+e^{-x}} \quad (2)$$

$$Y^{\tan sig} = \frac{e^{x} - e^{-x}}{e^{x} + e^{-x}} \quad (3)$$

## Modelling the A-A rapidity distributions using ANN:-

The proposed neural network (ANN) model [11-15 and references there in] of rapidity distributions of $\pi^-$ and $\kappa^{\pm}$ mesons produced in central Pb-Pb collisions have three inputs and one output. The inputs are the centre of mass energy (√s), mass number of the projectile nuclei (A) and the rapidity (Y). The output is the rapidity distribution dN/dY of $\pi^-$ and $\kappa^{\pm}$ mesons. By using this input output arrangement different network configurations were tried to achieve good mean square error (MSE) and good performance for network.

### Pseudo-rapidity Distributions of $\pi^-$ meson production in the central Pb+Pb collisions

The proposed neural network model of pseudo-rapidity distributions for $\pi^-$ produced in the central Pb+Pb collisions at (20, 30, 40, 80 and 160 A GeV respectively) have three inputs ($A$, $Y$, $\sqrt{S}$) one output ($dN/dy$) and two hidden layers (one layer consists of 7 neurons and the second consists of 5 neurons). The configuration of proposed ANN model shown in figure (3). The transfer function of the first layer and two hidden layers were chosen to be a tan sigmoid, while the output was chosen to be pure line.

The proposed ANN in the present work was trained using Levenberge-Marquradt optimization technique [11 - 13]. The optimization technique is more powerful than the conventional gradient descent technique. The Levenberge-Marquradt updates the network weights using the following rule:

$$\Delta W = (J^T J + \mu I)^{-1} J^T e \quad (4)$$

where J is the Jacobian matrix, e is a vector of ANN errors, μ is scalar, changed adaptively by the algorithm, and I is identity matrix.

The net which used in this work is the feed forward neural network back propagation. The trained method which used to train the ANN model is Levenberg-Marquardt optimization technique, with number of epochs = 112, and momentum = 1. In this case the center of mass energies (20, 30, 40 and 160 A GeV respectively) are used to train neural network model.

The training procedure is shown in figure (4). The plot shows the mean squared error of the network starting at a large value and decreasing to a smaller value. It shows the network is learning. The plot has three lines, because the input and target vectors are randomly divided into three set. 80% of the vectors are used to train the network. 20% of the vectors are used to validate how well the

network generalized. Training on the training vectors continues as long the training reduces the network's error on the validation vector. After the network memorizes the training set, training is stopped. This technique automatically [14, 15] avoids the problem of over fitting, which plagues many optimization and learning algorithms. Finally the last 20% of the vectors provide an independent test of the network generalization to data that the network has never seen.

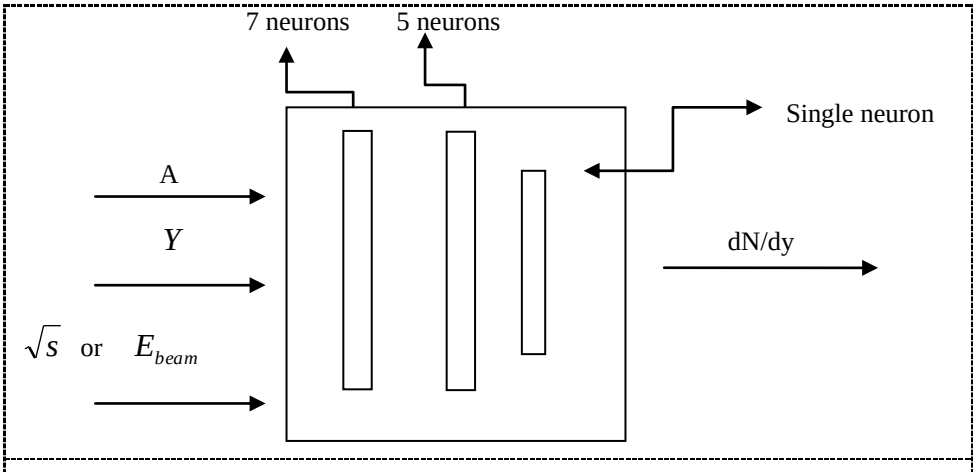


**Fig. 3.** A block diagram for $\pi^-$ produced in Pb+Pb collisions based on ANN model.

A very good agreement between the predicted values from the trained neural network and the validating data is achieved, which indicates that the trained network takes on optimal generalization performance. This also demonstrates, as a typical data mining technique, neural networks can find the basic pattern information implied in a great number of experimental data, extract useful rules and then apply these rules and then apply these rules to obtain reasonable predicted results.

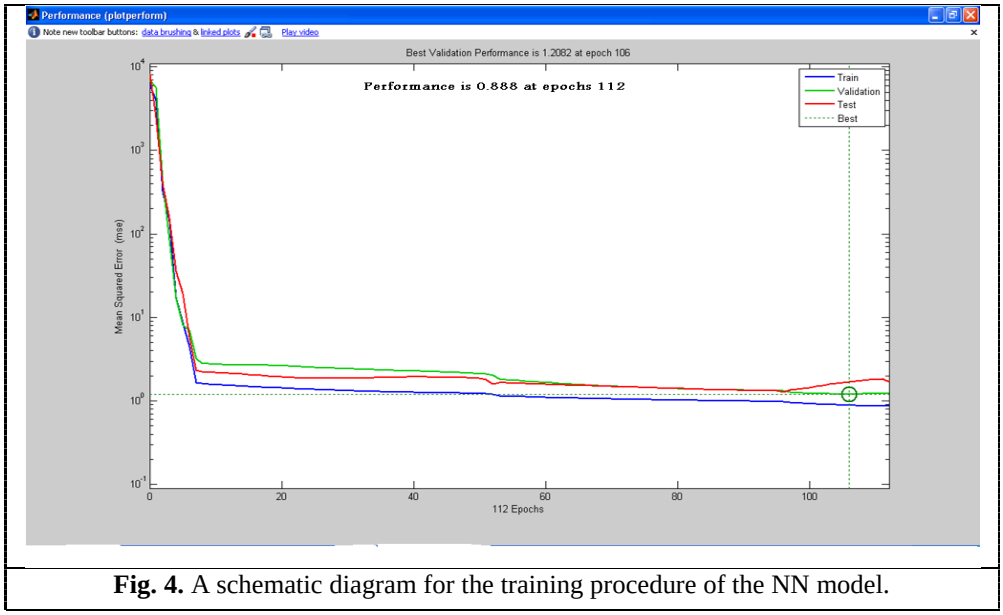


**Fig. 4.** A schematic diagram for the training procedure of the NN model.

The pseudo-rapidity distribution of $\pi^-$ produced in central (7% at 20-80 AGeV), (5% at 158 AGeV) at SPS energies ( experimental data) and the calculated results (solid lines) are obtained using the ANN model has been depicted in figure (5). Based on the present simulations it is clear that the calculated results are in good agreement with the experimental data [11-13 and references there in].

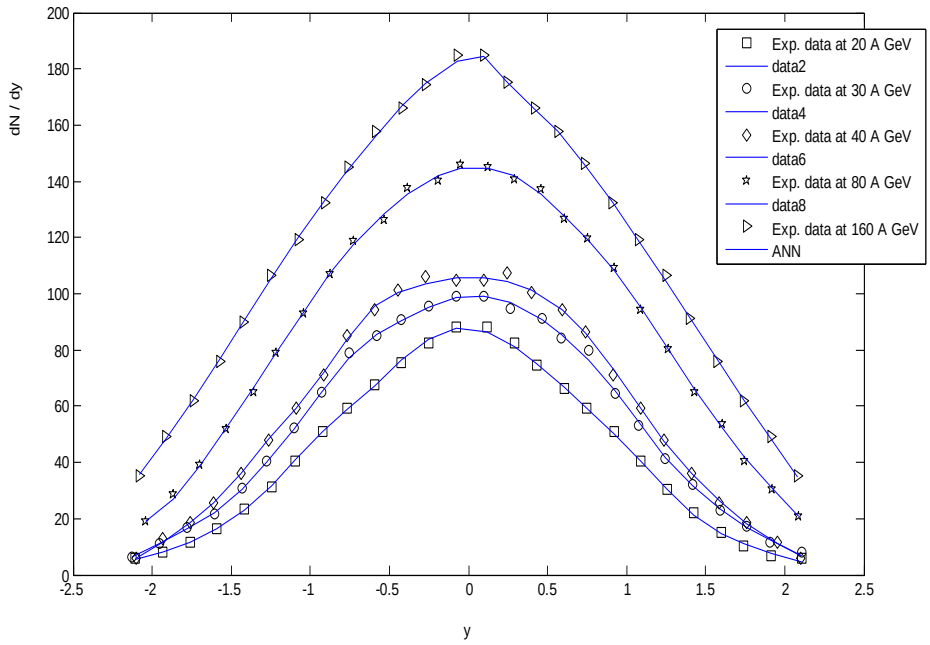


**Fig. 5:** Pseudo-rapidity distribution of $\pi^-$ in Pb-Pb collisions at SPS energies from 20 to 158A GeV (7% most central collisions for 20-80A GeV, 5% most central collisions for 158A GeV ) measured by the NA49 collaboration. [(o) Experimental data, (-) ANN].

The Pseudo-rapidity distribution of $\pi^-$ produced in central Pb-Pb collisions which obtained from ANN model is:

$$dN/dy = pureline[\{net.LW(3,2).\tan sigmoid.\{net.LW(2,1).\tan sigmoid\{net.IW(1,1).P + net.b(1)\} + net.b(2)\} + net.b(3)\}] \quad (5)$$

where,

$P$ is the input which is ( $A, y, E_{beam}$).

$net.LW(3,2)$ linked weight between the second hidden layer and the output.

$net.LW(2,1)$ linked weights between the first and the second hidden layer.

$net.IW(1,1)$ linked weights between the input layer and the first hidden layer.

$net.b(1)$ is the bias of the first hidden layer.

$net.b(2)$ is the bias of the second hidden layer.

$net.b(3)$ is the bias of the output layer.

The weights and biases in equation (5) are given in appendix A.

## Results and Discussions:-

### Multiplicity distributions of black, grey and heavy track producing particles

When an energetic projectile collides with a nucleus, a number of charged and uncharged particles are produced. The emission of these particles occurs in a short time after the impact of the impact of the projectile and thus the nucleus remains excited for quite a long time on nuclear time scale. The nucleus then de-excites resulting in emission of large number of nucleons and other heavy fragments. The particles emitted through this process of evaporation appear as black tracks in nuclear emulsion except for few grey tracks.
The multiplicity distributions of black, grey and heavily ionizing particles produced in $^{28}$Si+emulsion interaction at 14.6 A GeV/c is shown in figure 6 (a-c). It is clearly observed from these figures that in nucleus– nucleus collisions, the positions of the peaks of distribution appear in lower values of $N_b$, $N_g$, and $N_h$. Similar distributions have been reported for $^{28}$Si+emulsion interactions [16] and other projectiles at different energies [17-21], which indicate that the target associated particles, are characterized by a weak dependence on the projectile mass number ($A_p$). This result is consistent with those obtained by other workers [22 - 24]. The ranges of these distributions are found to be extended up to larger values of these parameters in case of heavier projectiles. The Numbers of hidden layers and neurons in all the multiplicity distributions of (Figure 6(a-c)) have been depicted in figure 7(a-c) and their details are such as (a) black tracks; Number of hidden layers and neurons 13 and 11, (b) grey tracks; Number of hidden layers and neurons 9 and 7 and (c) heavily ionizing tracks; Number of hidden layers and neurons 11 and 9 respectively.

### Multiplicity distribution of shower particles:

Figure 8, shows the multiplicity distribution of shower particles ($\beta > 0.7$) for $^{28}$Si+emulsion interactions at 14.6A GeV. It is evident from the figure that the tail of distribution extends to large values of Ns at 14.6 A GeV/c in $^{28}$Si+Em interactions. It can be concluded that number of relativistic charged particles produced increases with increasing energy of projectile, there by confirming the conversion of energy into mass. The values of $<N_S>$ and $<N_S>/D$ ($N_S$) have been calculated for our data, which comes out to be $18.02 \pm 0.26$ and $1.35 \pm 0.08$ respectively. The comparison of this result with others at different energies shows that $<N_S>/D$ remains practically independent of energy and projectile. Similar results reported in hadron – nucleus interactions [23, 24] indicate that the mechanism of shower particles production may be same for different types of collisions. In Fig. 9, the Number of hidden layers and neurons has been shown of figure 8, and found of the order of 11 and 9 respectively by ANN simulations.

The values of $<N_b>$, $<N_g>$ and $<N_S>$ for the present data are found to be $4.86 \pm 0.13$, $2.88 \pm 0.10$ and $18.02 \pm 0.26$ respectively. The comparison with other results [7, 8, 22-27] gives an indication that the values of $<N_g>$ increase slightly with the incident beam energy as well as with projectile mass. The values of $<N_b>$ do not exhibit any such behaviour. On the other hand, the $<N_S>$ is observed to increase with increasing projectile mass as well as energy of the projectiles.

The multiplicity distribution of total charged secondary particles $N_{ch}$ ($N_{ch} = N_b + N_g + N_S$) is displayed in figure 10 for Silicon beam at 14.6A GeV. The tails of total charged secondary particles distributions are found to extend up-to high multiplicities of $N_{ch} = 256$. The long tail of the distributions may arise from the interactions of all the nucleons present in the projectiles with the target nucleus, which is ultimately possible due to the transfer of projectile energy to the total nuclei. In Fig. 11, the Number of hidden layers and neurons has been shown of figure 10, and found of the order of 3 and 2 respectively by ANN simulations.

#### Angular Distribution of Relativistic Shower Particles

The angular distribution of relativistic shower particles produced in $^{28}$Si-emulsion collisions is shown in Fig. 12. It is evident from the figure that most of the shower particles are produced in the forward direction. Thus, it seems that shower particles produced in high-energy interactions are highly collimated in the forward direction. The forward to backward (F/B) ratio comes out to be $51^{\circ} \pm 2.1$.

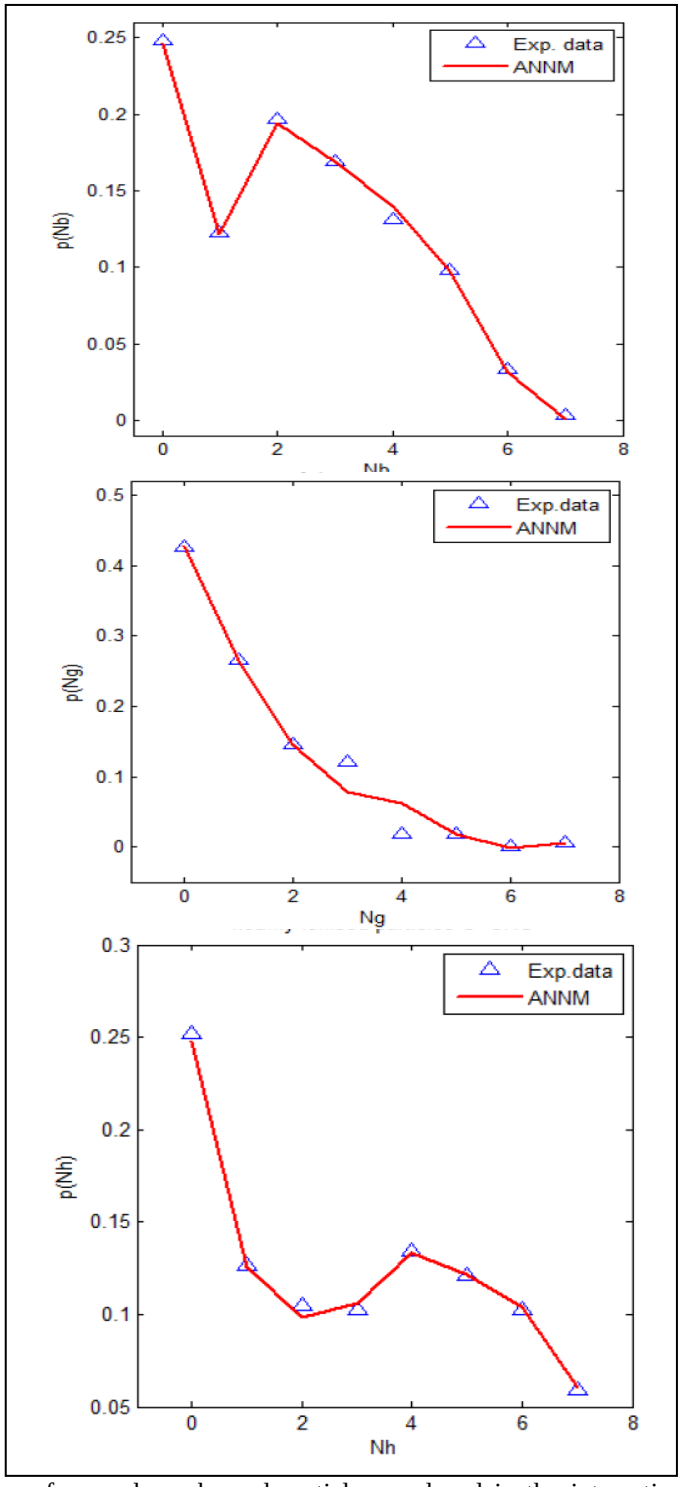


**Fig. 6(a-c).** Multiplicity distributions of secondary charged particles produced in the interactions of $^{28}$Si-Em at 14.6A GeV for (a) black tracks (b) grey tracks and (c) heavily ionizing tracks.

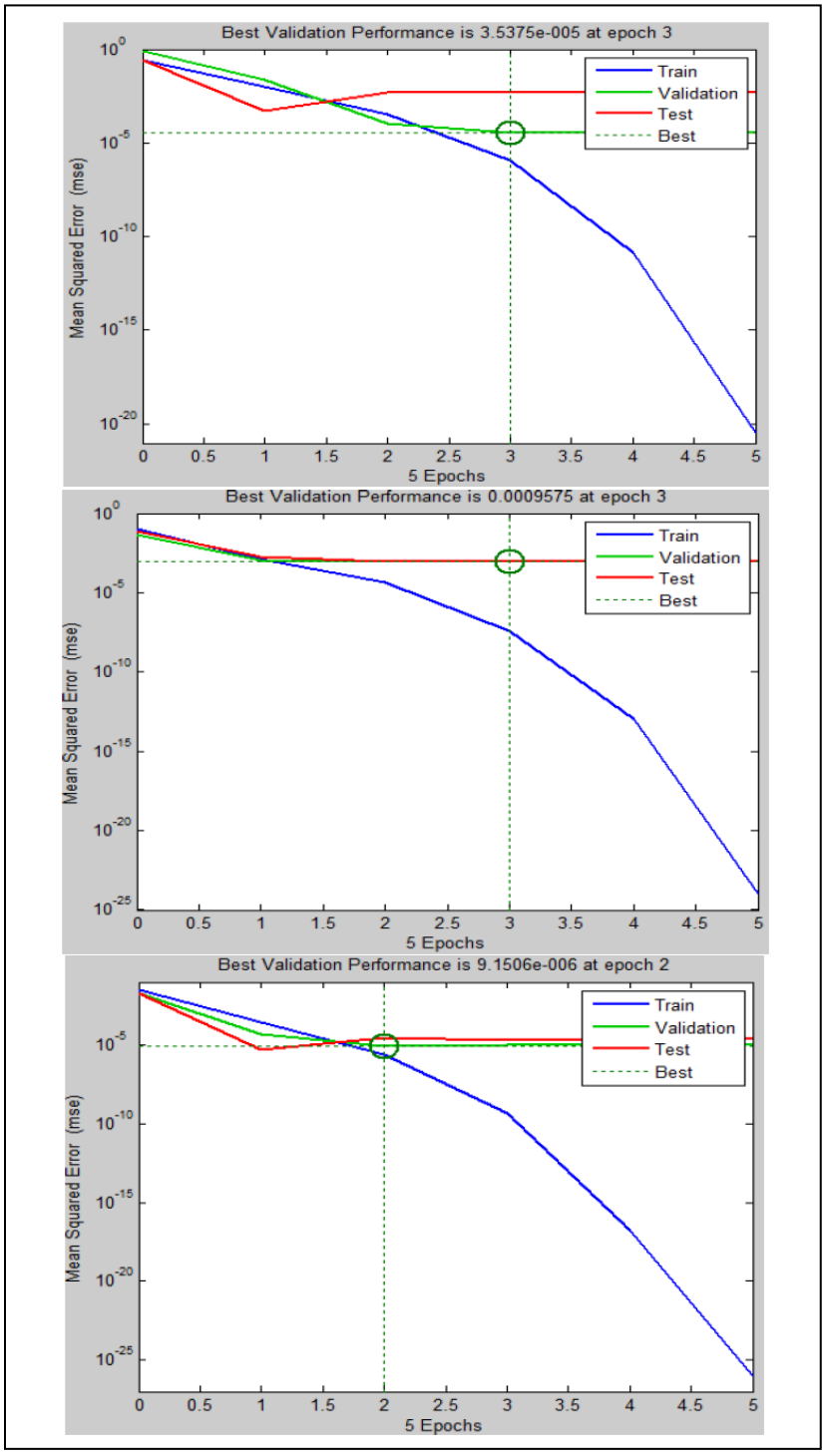


**Fig. 7(a-c).** Number of hidden layers and neurons in all multiplicity distributions of Fig.6 (a-c) for (a) black tracks (b) grey tracks and (c) heavily ionizing tracks.

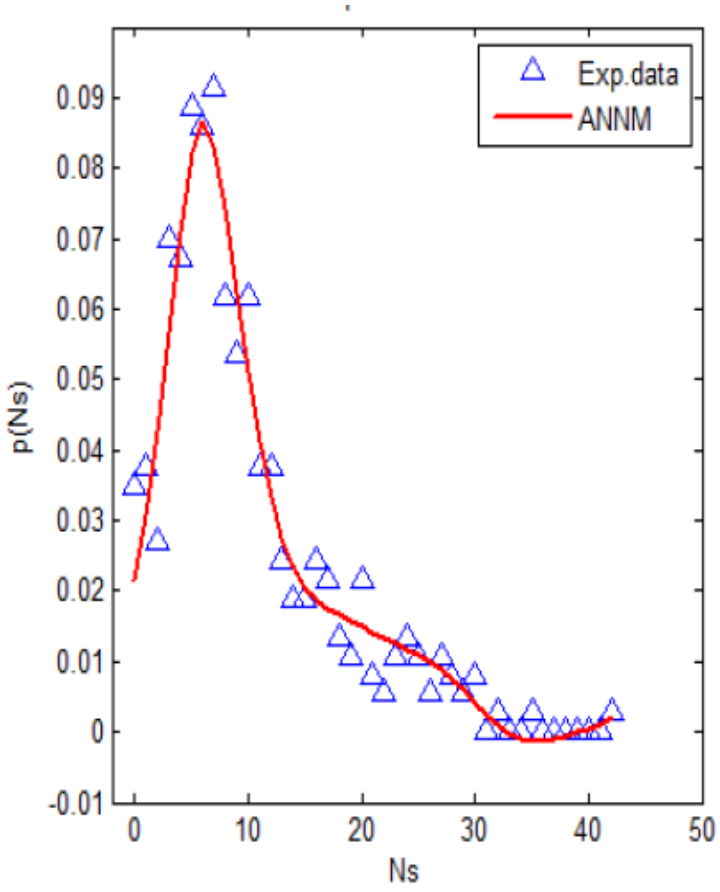


**Fig. 8.** Shower particle multiplicity distributions in the interactions of $^{28}$Si-Em at 14.6A GeV.

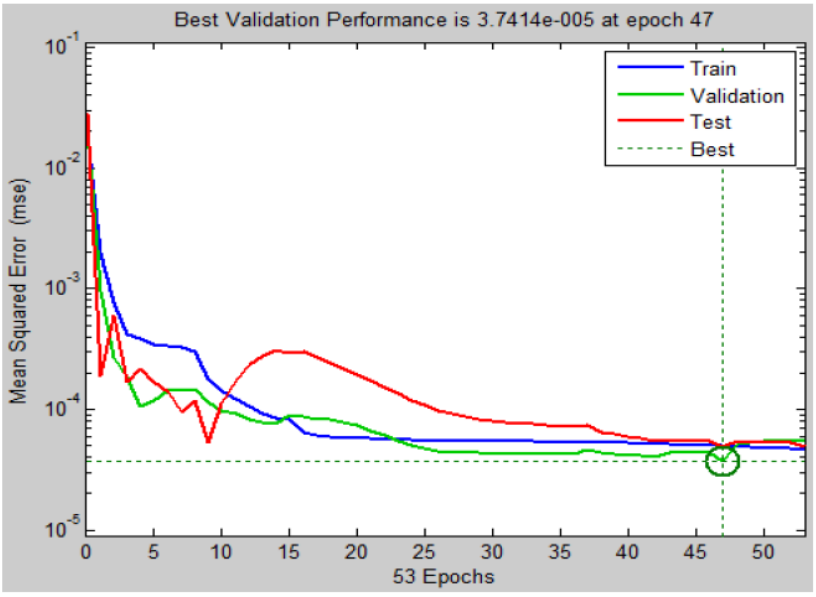


**Fig. 9.** The Number of hidden layers and neurons 11 and 9 respectively of Figure 8.

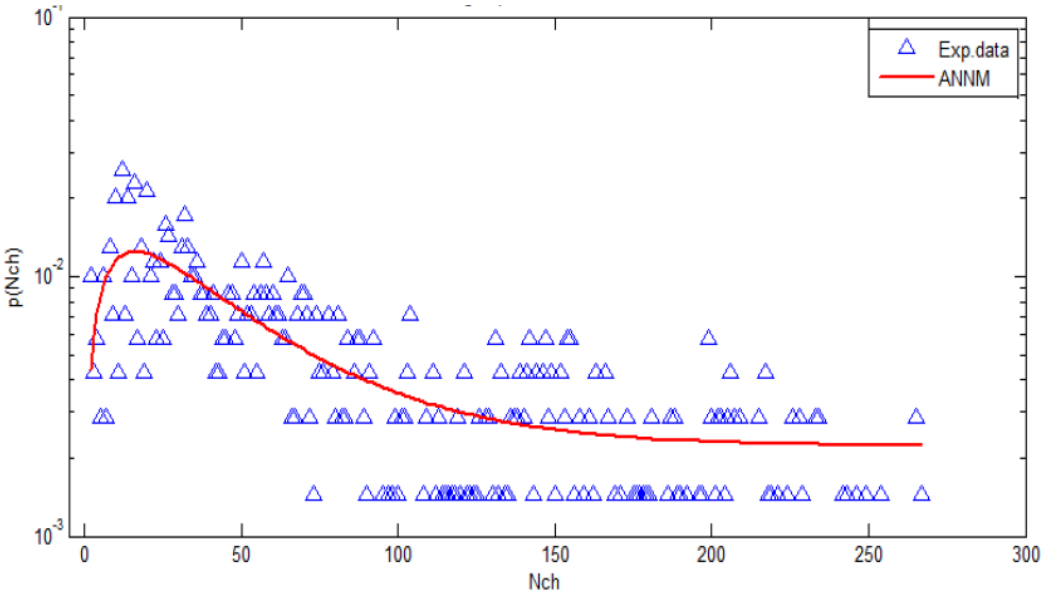


**Fig. 10.** Total charge ($N_{ch}$) multiplicity distributions in the interactions of $^{28}$Si-Em at 14.6A GeV.

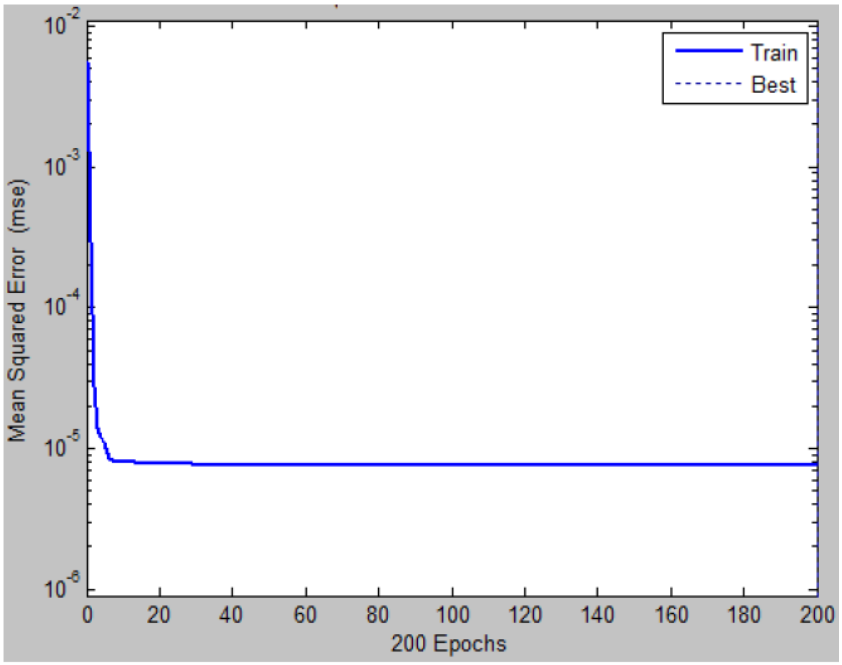


**Fig. 11.** The Number of hidden layers and neurons 3 and 2 respectively of Figure 10.

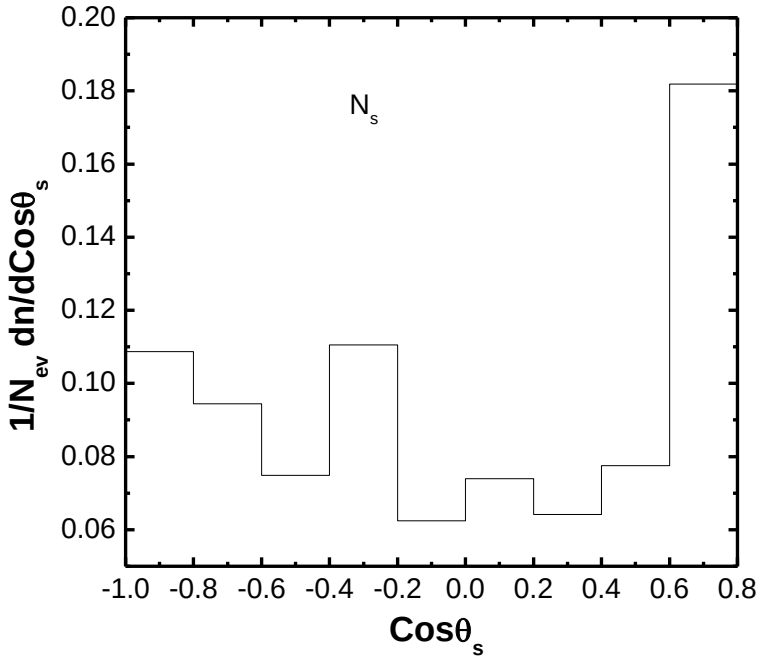


**Fig. 12.** Angular distribution of relativistic shower particles produced in the interaction of $^{28}$Si-emulsion at 14.6A GeV.

## Multiplicity correlations between various particles

It is well established that shower and gray tracks producing particles characterize the first stage of the inelastic collision between the two nuclei and black track producing particles correspond to the next stage of the collision when the de-excitation process occurs through the evaporation of nucleons. A linear dependence between multiplicities of different particles has been observed, which can be represented by the following relations:

$$< n_i (n_j) > = a_{ij} + b_{ij}, \qquad a_{ij} > 0 \quad \text{.....(5)}$$

where $a_{ij}$ and $b_{ij}$ depends on the incident energy and mass of projectile ($n_i$ and $n_j$ stand for $N_b$, $N_g$ and $N_S$ ). The multiplicity correlations of secondary particles produced in nucleus-nucleus collisions at 14.6A GeV have been studied. These results are shown in Fig 13 (a-d) along with their linear fits shown by solid lines in the figures.
The following conclusions are drawn from these figures:

**(i) Dependence of $<N_g>$, $<N_h>$ and $<N_S>$ on $N_b$**

We have investigated the dependence of $<N_g>$, $<N_h>$ and $<N_S>$ on $N_b$ for total data in Fig 13 (a). The following relations have been obtained:

$$<N_g> = (0.470 \pm 0.023)\ N_b + 0.661 \pm 0.106 \text{.....(5.1a)}$$

$$<N_h> = (1.188 \pm 0.059)\ N_b + 12.475 \pm 0.336 \text{.....(5.1b)}$$

$$<N_S> = (1.490 \pm 0.033)\ N_b + 0.660 \pm 0.119 \text{.....(5.1c)}$$

**(ii) Dependence of $<N_b>$, $<N_h>$ and $<N_S>$ on $N_g$**

The variation of $<N_b>$, $<N_h>$ and $<N_S>$ with $N_g$ has been given in Fig. 13 (b) for total data, which satisfy the following relationships:

$$<N_b> = (1.033 \pm 0.058)\ N_g + 1.957 \pm 0.154 \text{.....(5.2a)}$$

$$<N_S> = (1.991 \pm 0.102)\ N_g + 12.643 \pm 0.351 \text{.....(5.2b)}$$

$$<N_h> = (2.054 \pm 0.073)\ N_g + 1.942 \pm 0.164 \text{.....(5.2c)}$$

**(iii) Variation of $<N_b>$, $<N_g>$ and $<N_S>$ on $N_h$**

The variation of $< N_b >$, $< N_g >$ and $< N_S >$ with $N_h$ has been given in Fig. 13 ( c) for the total data, which satisfy the following relationships:

$$<N_b> = (0.659 \pm 0.019)\ N_h + 0.083 \pm 0.136 \text{.....(5.3a)}$$

$$<N_g> = (0.077 \pm 0.014)\ N_h + 0.080 \pm 0.100 \text{.....(5.3b)}$$

$$\langle N_S \rangle = (0.950\pm0.040)\ N_h + 10.742\pm0.199 \quad \text{(5.3c)}$$

**(iv) Dependence of $\langle N_b \rangle$, $\langle N_g \rangle$ and $\langle N_h \rangle$ on $N_S$**

The dependence of $\langle N_b \rangle$, $\langle N_g \rangle$ and $\langle N_h \rangle$ on $N_S$ has been given in Fig. 13 (d). These exists a linear relationship between $< N_b >$, $< N_g >$ and $< N_h >$ on $N_S$, which satisfy the following relationships.

$$\langle N_b \rangle = (0.220\pm 0.029)\ N_S + 0.096 \pm 0.461 \quad \text{(5.4a)}$$

$$\langle N_g \rangle = (0.169\pm 0.023)\ N_S + 0.011 \pm 0.355 \quad \text{(5.4b)}$$

$$\langle N_h \rangle = (0.375\pm 0.037)\ N_S + 1.196 \pm 0.605 \quad \text{(5.4c)}$$

The following important features may be noted from these dependences:

(i) It is evident from the above figures that the values of $\langle N_S \rangle$ increase with increasing values of $N_b$, $N_g$ and $N_h$. However, no such positive correlation is reported for p-Em collision [24,25, 28].

(ii) For the present data, the values of $\langle N_b \rangle$ have been found to increase with $N_S$, where as no such behavior is observed in p-Em collisions. In case of $< N_b >$ vs. $N_g$ plots, a saturation is observed around $N_g \sim 9$. Similar result has been observed for π-Em and p-Em interactions at 200 and 400 GeV [23, 27-29] respectively.

(iii) The values of $\langle N_S \rangle$ at fixed $N_b$, $N_g$ and $N_h$ are always larger for nucleus-nucleus collisions than for hadron-nucleus collisions.

(iv) A linear increase has been found in the dependences of $\langle N_b \rangle$, $\langle N_g \rangle$ and $\langle N_S \rangle$ on $N_h$, where as a strong correlation between $\langle N_b \rangle$and $\langle N_g \rangle$ has been found and there is a negative correlation between $\langle N_S \rangle$ vs. $N_h$ in p-Em interactions.

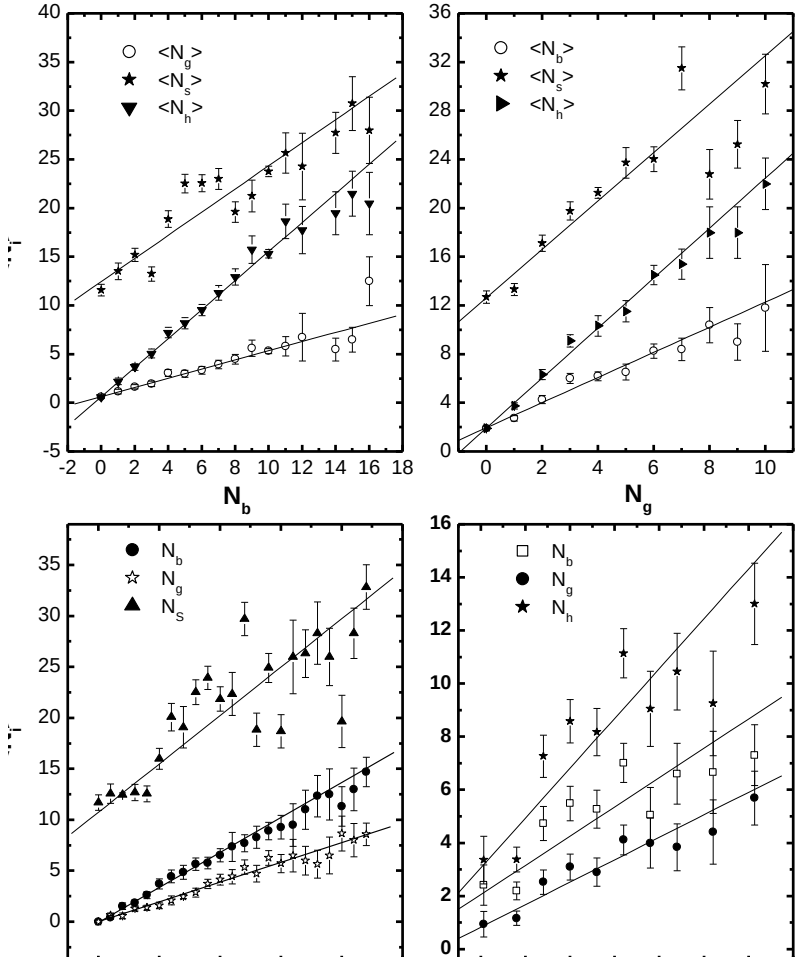


**Fig. 13 (a-d).** Multiplicity correlations of various charged particles produced in the interactions of $^{28}$Si-Em at 14.6A GeV.

## 5. Outcomes of Present Study

Some significant results have been obtained for multi-particle production in the present work. It is believed that multiplicity fluctuations and correlations may be a weak signal of QGP formation in such experiment. Further, evidence of these multiplicities correlations has also been observed in low energy nuclear collisions, whereas the formation of QGP is not expected. So far, QGP phase transition cannot be the only reason for the fluctuations observed in present experimental data. It may be possible that the observed fluctuations / correlations may have more remarkable explanation.

The tail of the shower particle distribution for all the projectiles, shifts towards the higher values of $N_S$ with the increase in projectile energy, thereby confirming production of more relativistic shower particles within the increasing incident energy, these may be suitable candidates for the observation of quark gluon plasma.

The mean multiplicity of shower particles, $<N_S>$, as well as compound track producing particles, $<N_c>$, and total charged particles $<N_{ch}>$ increases, as mass number of the projectiles increases. However the mean multiplicity of black particles, $<N_b>$, is essentially unchanged, whereas a little change in the mean multiplicity of grey particles, $<N_g>$, is observed with increase in mass of the projectiles. The multiplicity correlations of secondary particles produced in nucleus-nucleus collisions are similar to hadron-nucleus collisions and could be represented by a linear dependence. A strong correlation between the number of shower tracks, $<N_S>$, and grey tracks, $N_g$, has been observed. There exists a clear saturation in the values of $<N_b>$ vs. $N_g$ plots beyond certain values of $N_g$.

Finally, from the study of correlation, it is evident that a short-range correlation is observed whereas there is a poor indication for the long-range correlation.

## Acknowledgment:-

The authors would like to acknowledge financial support for this work from the Deanship of Scientific Research (DSR), University of Tabuk, Tabuk, Saudi Arabia, under grant no. S-00236-1436 [30-32].

## References:-

**[1]. Miklos Gyulassy, (1984).** Signatures of new phenomena in ultrarelativistic nuclear collisions. Nuclear Physics. A418**:** 59-85 (1984).

**[2]. M. Stephanov et al., (1991).** Event-by-Event fluctuations in heavy ion collisions and the QCD crititical point - art. No. 114028. Physical. Review. D60 (11): pp. 4028.

**[3]. Shafiq Ahmad, M. Ayaz Ahmad (2006**). A comparative study of multifractal moments in relativistic heavy-ion collisions. Journal of Physics G Nuclear and Particle Physics. 32(9):1279-1293.

**[4]. S. A. Bass et. al., (1998).** Microscopic Models for Ultrarelativistic Heavy Ion Collisions. Prog .Part. Nucl. Phys. 41: 255-369 arXiv:nucl-th/9803035v2

**[5]. J. D. Bjorken. (1983).** Highly relativistic nucleus-nucleus collisions: The central rapidity region. Physical Review. D27: 140-151.

**[6]. Mir Hashim Rasool, M. Ayaz Ahmad and Shafiq Ahmad. (2015).** Multifractal study and multifractal specific heat of singly charged particles produced in 32S-Em interactions at 200AGeV. Chaos Solitons & Fractals. 81: 197-202. DOI:10.1016/j.chaos.2015.08.027

**[7]. Mir Hashim Rasool, M. Ayaz Ahmad, M. Ahmad Bhat and Shafiq Ahmad. (2015).** Study of Compound Particle Production in $^{28}$Si and $^{32}$S-Emulsion Collisions at 14.6 and 200 AGeV. World Journal of Nuclear Science and Technology. 5(03): 208-220. DOI:10.4236/wjnst.2015.53021

**[8]. Mir Hashim Rasool, M. Ayaz Ahmad, Omveer Singh and Shafiq Ahmad. (2015).** Some Important Features of Relativistic Charged Particles Produced in 32S-Emulsion Interactions at 200 AGeV/c. Journal of Modern Physics. 6:1498-1509. DOI:10.4236/jmp.2015.611154

**[9]. M. Ayaz Ahmad, Mir Hashim Rasool, Shafiq Ahmad, Jamal H. Madani and Rachid Ayad (2013)**. Study of Deconfinement Phase Transition in Heavy Ion Collisions at BNL Energies. International Journal of Applied Physics and Mathematics, (IJAPM). 4: 289-292. DOI: 10.7763/IJAPM.2013.V3.223

**[10]. M. Ayaz Ahmad, Mir Hashim Rasool and Shafiq Ahmad. (2013).** Scaling nature of target fragments in the interactions of 28Siemulsion at energy 14.6A GeV. Ukrainian Journal of Physics. 58(10): 944-955.

**[11]. El-Bakry Mostafa Y., El-Harby A. A. and Behery G. M. (2008).** Automatic Neural Network System for Vorticity of Square Cylinders With Different Corner Radii. Journal of Applied Mathematics And Informative (JAMI). 26(5-6): 911-923.

**[12]. Elbakry Mostafa Y. and Radi A., (2007).** Genetic Programming Approach for flow of steady state fluid between two eccentric spheres, Appl. Rheol. 17(6): 68210.

**[13]. El Bakry M.Y., and El-Metwally K. A. (2003)**. Neural Network for Proton- Proton Collision at High Energy. Chaos, Solutions and Fractals. 16(2): 279-285.

**[14]. Alveera Khan, M. Ayaz Ahmad, S. Joshi. (2015).** A systematic study for electrical properties of chemically treated coir fiber reinforced epoxy composites with ANN model. International Journal of Science and Research (IJSR). 4(1): 410-414.

**[15]. Vesna K. Hristova, M. Ayaz Ahmad, Biljana Trajkovska, Stefce Presilski, Georgi Bonev. (2015).** Artificial Neural Networking Model an Approach for the Coagulation Properties of Milk. International Journal of Scientific and Engineering Research (IJSER). 6(4): 1117-1121.

**[16]. M. Tariq, M. Ayaz Ahmad, Shafiq Ahmad, M. Zafar. (2007).** Analysis of high Ns -multiplicity events produced in relativistic heavy ion collisions at 4.5 A GeV/c. Romanian Reports in Physics. 59(3): 773-790.

**[17]. M. Ayaz Ahmad and Shafiq Ahmad (2012).** Study of Angular Distribution and KNO Scaling in the Collisions of $^{28}$Si with
Emulsion Nuclei at 14.6A GeV. Ukrainian Journal of Physics. 57(12): 1205-1213.

**[18]. G. J. Alner, K. Alpgard, P. Anderer et al., (1987).** UA5: A general study of proton-antiproton physics at $\sqrt{s}$ = 546GeV. Physics Reports. 154(5-6): 247–283.

**[19]. N. N. Abd Allah and M. Mohery. (2001).** Features of the compound multiplicity of the interactions of $^{24}$Mg and $^{28}$Si ions with emulsion nuclei at 4.5 A GeV/c. Turkish Journal of Physics. 25:109-119.

**[20]. Z. Abou Moussa. (2002).** Compound multiplicity in the collisions of 4.1 A GeV/c $^{22}$Ne nuclei with nuclear emulsion. Canadian Journal of Physics. 80: 109-117.

**[21]. D.-H. Zhang, C.-L. He, Y. Yuan et al., (2006**). Features of compound multiplicity in $^{16}$O-Em interactions at 4.5 A GeV/c. Chinese Journal of Physics. 44: 405-417.

**[22]. Shafiq Ahmad, M. Ayaz Ahmad, M. Tariq and M. Zafar. (2009).** Charged multiplicity distribution in relativistic heavy-ion collisions. International Journal of Modern Physics E18(09): 1929-1944.
DOI:10.1142/S0218301309013968

**[23]. M. El-Nadi, O. E. Badawy, M. K. Hegab et al,. (1983).** Inelastic interactions of 340 GeV/c π- with emulsion nuclei, Physical Review. D27: 12-18.

**[24]. R. K. Shivpuri and A. Kotha. (1987)**. Multiplicity, rapidity and rapidity correlations in 800 GeV proton-nucleus interactions, Physical Review. D35: 3508-3511.

**[25]. I. Otterlund, E. Stenlund, B. Andersson and G. Nilson. (1978)**. Nuclear interactions of 400-GeV protons in emulsion, Nuclear Physics. B142: 445-462.

**[26**] V. E. Dudkin et al, (1990). Multiplicities of secondaries in interactions of 1.8 GeV/nucleon $^{56}$Fe nuclei with photoemulsion and the cascade evaporations model. Nuclear Physics. A509: 783-791.

**[27]. M. Mohery and M. Arafa. (2011).** Some characteristics of the compound multiplicity in high-energy nucleus-nucleus interactions, International Journal of Modern Physics E20: 1735-1754.

**[28]. C.-Y. Bai and D.-H. Zhang. (2011).** Study of compound particle production in $^{84}$Kr-emulsion interactions at 1.7 A GeV. Chinese Physics. C35: 349-354.

**[29]. Z. V. Anzon et al (Alma Ata-Leningrad-Moscow-Tashkent Collaboration). (1977).** A study of inelastic pion-nucleus interactions at 200 GeV/c in an emulsion. Nuclear Physics. B129: 205-234.

**[30]. Anghel Drugarin Cornelia Victoria, M. Ayaz Ahmad, N. Ameer Ahmad, Draghic Silviu. (2015).** The Mathematical Study of Data Transmission in Digital Electronics. International Journal of Advanced Research (IJAR). 3(3): 697- 702.

**[31]. Anghel Drugarin Cornelia Victoria, M. Ayaz Ahmad, N. Ameer Ahmad, Vyacheslav V. Lyashenko. (2015).** Algorithmic Research and Application Using the Rayleigh Method", International Journal of Science & Research (IJSR). 4(4): 1669-1671.

**[32]. Dragos Pasculescu, Remus Dobra and M. Ayaz Ahmad (2016).** Dosimetric Quantity System for Electromagnetic Fields Bio-effects" article accepted for publication in International Journal of Scientific Research 2016.